Journal of the Serbian Chemical Society
JSCS-info@shd.org.rs • www.shd.org.rs/JSCS
J. Serb. Chem. Soc. *87* (9) 1011–1024 (2022)
JSCS–5574
Original scientific paper
Published 1 August 2022

Advanced dye removal by multifunctional layered double hydroxide based materials: Adsorption and kinetic studies

MILICA S. HADNAĐEV-KOSTIĆ*#, TATJANA J. VULIĆ, ĐURĐICA M. KARANOVIĆ# and MARIJA M. MILANOVIĆ

Faculty of Technology Novi Sad, University of Novi Sad, bul. Cara Lazara 1, 21000 Novi Sad, Serbia

(Received 28 February, revised 1 April, accepted 8 April 2022)

Abstract: Due to favourable properties layered double hydroxides (LDHs) have been widely investigated for organic dye removal processes. In order to study the adsorption of methyl orange, bimetal (ZnAl and MgAl) and trimetal (ZnCuAl and MgCuAl) adsorbents were synthesized and thermally treated. The influence of adsorbent metal nature and content on structural (X-ray diffraction, Raman analysis), textural (low temperature nitrogen adsorption) and adsorption properties was investigated. Adsorption behaviour, mechanisms, and stability of synthesized LDHs and their calcined mixed oxides were studied with the aim to elucidate the adsorbent-dye interactions, enabling optimization of experimental design. All LDH adsorbents and LDH derived mixed oxide adsorbents had high removal efficiency rate, especially Zn-containing mixed oxides where complete decolourization (100 % of dye removal) was achieved almost instantly due to super-fast adsorbent-adsorbate interaction. Two possible adsorption mechanisms initiated by interfacial phenomena were in correlation with the structural and textural properties, as well as with the "memory effect" reconstruction phenomenon. These results present a solid base for further investigation and design of LDH-based adsorbents for the Methyl orange removal, considering their favourable structural and textural properties and excellent adsorption capacities.

Keywords: anionic clays; LDH derived mixed oxides; methyl orange removal; wastewater treatment.

INTRODUCTION

Water contamination by various organic dye pollutants has become a major concern on a global scale, considering the impact on the environment and public health.[1] Organic dyes are aesthetic pollutants that provoke water colorization

* Corresponding author. E-mail: hadnadjev@tf.uns.ac.rs
# Serbian Chemical Society member.
https://doi.org/10.2298/JSC220228034H

inhibiting light penetration and causing short- and long-term changes in the ecosystems. One of the most commonly industry generated dye is methyl orange (MO), a well-known water-soluble anionic dye with pronounced carcinogenic and toxic character.[2] Therefore, the research community agrees on the imperative to develop a rapid and effective approach for dye removal from water. Adsorption is defined as a reliable alternative that is cost-effective, simple in design and operation and highly efficient for dye removal from contaminated water.[3] Since the adsorption process involves complex interfacial phenomena, for stable and effective use of adsorption, it is necessary to have a detailed understanding of kinetics and mechanisms of each specific adsorption process. Considering the importance of MO removal from the environment, there is a continuous need for novel adsorbents with adequate surface charge, high adsorption capacity and removal efficiency. Recently, layered double hydroxides (LDHs) have been studied as adsorbents considering their initial cost, ease of operation and satisfactory adsorption capacity.[4] These materials are a versatile class of two-dimensional ionic laminar compounds, with octahedral brucite-like ($Mg(OH)_2$) layers containing bimetal and trimetal cations with anions (CO_3^{2-}, NO_3^-, Cl^-) and water embedded between hydroxide sheets.[2,5] After calcination (450–500 °C) the layered structure collapses producing non-stoichiometric mixed oxides that are characterized by high specific surface area, with the ability to reconstruct the original layered structure when exposed to air and aqueous solution, *i.e.*, memory effect.[6]

The motivation for this study was to: *i*) successfully synthesize M^{2+}–Al––LDHs and M^{2+}–CuAl–LDHs by the coprecipitation method; *ii*) investigate adsorption behaviour of synthesized LDHs and derived mixed-oxides; *iii*) elucidate adsorbent–adsorbate interactions enabling optimization of experimental design. Since the adsorption is a complex interfacial phenomenon, this study aims to promote better understanding of adsorption kinetics correlating structural, physicochemical and textural properties with adsorption removal process.

EXPERIMENTAL

Synthesis and preparation

LDH adsorbents were prepared using coprecipitation synthesis method at constant pH of 9.[5,6] Precursor solutions, from $Zn(NO_3)_2{\cdot}6H_2O$, $Mg(NO_3)_2{\cdot}6H_2O$, $Al(NO_3)_3{\cdot}9H_2O$ and $Cu(NO_3)_2{\cdot}6H_2O$, were added continuously (4 cm^3 min^{-1}; 40 °C), with the base solution (0.67 M Na_2CO_3; 2.25 M NaOH). The trivalent Al-ion concentration (30 mol %) and overall concentration of bivalent ions (70 mol %) remained the same. In case of trimetal LDHs, only 5 mol % of Zn or Mg was substituted by Cu. Precipitation products were aged (15 h), washed with distilled water until pH 7, dried (24 h; 100 °C) and calcined (5 h; 500 °C; in air). Dried samples were denoted as ZnAl–LDH, ZnCuAl–LDH, MgAl–LDH, MgCuAl–LDH and calcined samples as ZnAl–C, ZnCuAl–C, MgAl–C and MgCuAl–C.

Characterization

Crystalline phases were identified by X-ray powder diffraction (XRPD) using Rigaku MiniFlex 600 diffractometer (CuKα radiation, λ = 0.15406 nm; 2θ 10–70°; scan rate = 0.02 s^{-1}). The lattice parameters were calculated for the dominant phase. Average crystallite size, d_p, was estimated using Scherrer equation based on the peak full width at half intensity (FWMH):

$$d_p = \frac{0.9\lambda}{\beta \cos\theta} \quad (1)$$

where λ is X-ray wavelength, β is FWMH and θ is diffraction angle. Calcined samples after MO adsorption were also analysed and denoted as ZnAl–CMO, ZnCuAl–CMO, MgAl–CMO and MgCuAl–CMO.

The Raman spectra for LDH samples were obtained using Thermo Scientific DXR Raman microscope by excitation with the green laser light (532 nm) and wavenumber from 100 to 1500 cm^{-1}.

Low temperature nitrogen adsorption at –196 °C (Micromeritics ASAP2000) was used for textural characterization. The specific surface area and pore size distribution were calculated using BET and BJH methods.

Adsorption experiments

Adsorption was carried out in an open Pyrex vessel containing 100 ml of MO solutions (C_{MO} = 20 mg dm^{-3}) and 50 mg of adsorbent and vigorously stirred. At defined time intervals, MO concentrations were determined using the UV–Vis spectrophotometer (Cecil2000) at the maximum MO absorption wavelength (λ = 463.9 nm). MO removal efficiency (E_f / %) was calculated as:

$$E_f = 100\frac{C_0 - C_t}{C_0} \quad (2)$$

where C_0 and C_t, in mg dm^{-3}, are values for initial dye concentration and concentration at the defined time, *t*.

The adsorption kinetics was evaluated using the pseudo-second-order model:

$$\frac{t}{q_t} = \frac{1}{k_2 q_e^2} + \frac{1}{q_e} t \quad (3)$$

where q_e / mg g^{-1} and q_t / mg g^{-1} are adsorption capacities at equilibrium conditions and at defined time *t* / min; k_2 / g mg^{-1} min^{-1} is equilibrium rate constant. Adsorption parameters, q_e and k_2, were determined from the slope and intercept of plot for t/q_t *vs.* *t*.

The diffusion mechanism was investigated by the intra-particle diffusion (IPD):[2]

$$q_e = k_i t^{0.5} + C \quad (4)$$

where k_i / g mg^{-1} $min^{-0.5}$ is the IPD rate constant obtained from the slope and *C* is the intercept.

RESULTS AND DISCUSSION

Structural characterization

All LDHs exhibited structure with basal reflections of planes *hkl* (003) and (006), consisting of M^{2+}–M^{3+} hydroxide sheets and interlayers with anions and H_2O, as well as with non-basal reflections (012), (015), (018), (110) and (113), similar to the brucite structure, consistent with the typical LDH structure, Fig.

1a.[7] XRD patterns could be indexed as hexagonal structure with *R*3*m* rhombohedral space symmetry.[8]

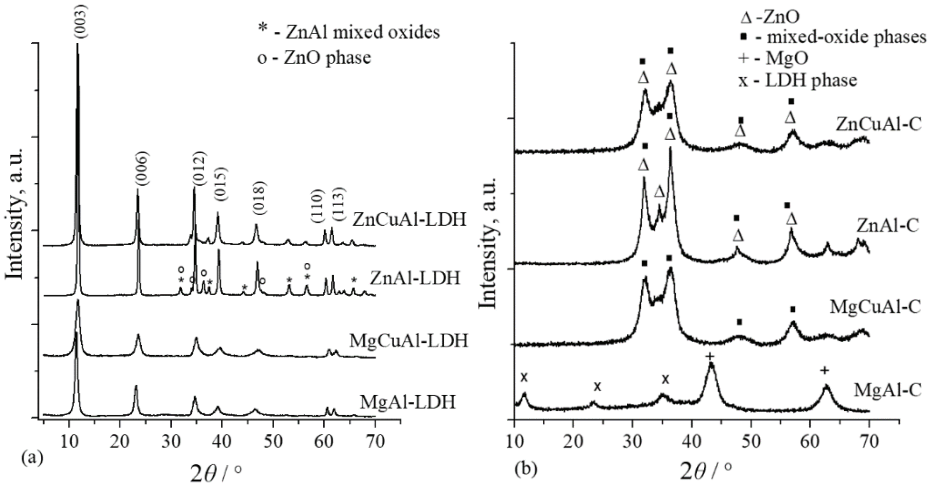

Fig. 1. XRD patterns for: a) LDHs and b) calcined samples.

Additional phases, ZnO and Zn(Al)O mixed oxides, were detected in Zn--samples.[9] A slight decrease in reflection intensity and sharpness was observed for Cu–LDHs, due to the Jahn–Teller distortion initiated by Cu incorporation into LDH structure.[10]

XRD analysis of calcined samples showed the collapse of the original LDH structure and formation of mixed oxides. For calcined Zn-samples, the most intense reflections indicated the presence of ZnO structure corresponding to (100), (002), (101) and (110) planes overlapping with Zn(Al)O mixed oxide phase.[11] MgAl–C sample revealed the presence of a cubic (NaCl-type) Periclase MgO phase[12] with three broad low intensity reflections corresponding to LDH phase and indicating incomplete LDH structure destruction. In MgCuAl–C sample CuO and Mg(AlCu)O mixed oxide phases were formed.[13] The lattice parameters of synthesized samples were defined for the dominant LDH phase and unit cell parameters were evaluated: *a* (width of crystal unit cell – cation–cation distance in brucite-like sheets), *c* (height of crystal unit cell) and *c*' (basal space – thickness of one layer consisting of a brucite-like sheet and one interlayer), average crystallite size and crystal lattice structure (Table I).

Structural parameters for the dominant LDH phase were calculated as:[6,14]

$$a = 2d_{110} \quad (5)$$

$$c = 3d_{003} = 3c' \quad (6)$$

TABLE I. Lattice parameters, crystal structure and specific surface area of LDHs and CMOs

Parameter	ZnAl–LDH	ZnCuAl–LDH	MgAl–LDH	MgCuAl–LDH	ZnAl–CMO	ZnCuAl–CMO	MgAl–CMO	MgCuAl–CMO
$d_{003} = c'$ / nm	0.7469	0.7545	0.7682	0.7564	0.7603	0.7603	0.7662	0.7487
d_{006} / nm	0.3757	0.3786	0.3839	0.3762	0.3794	0.3786	0.3839	0.3757
d_{110} / nm	0.1532	0.1538	0.1526	0.1518	0.1537	0.1537	0.1526	0.1518
a / nm	0.3064	0.3076	0.3051	0.3036	0.3075	0.3073	0.3053	0.3036
c / nm	2.2401	2.2634	2.3046	2.2692	2.2809	2.2809	2.2986	2.2462
Interlayer thickness, nm	0.2668	0.2745	0.2882	0.2764	0.2803	0.2803	0.2862	0.2687
d_p / nm	25.36	19.58	13.78	10.15	25.88	20.1	13.4	9.97
S / m^2 g^{-1}	22.98	32.5	57.2	72.7	–	–	–	–

The d_{003} values were twice as high as d_{006} suggesting a favourable stacking of layers in the layered structure.[15] A mild difference in a value for Cu–LDHs was observed, being slightly higher after Cu cation in Zn-samples and slightly lower after Cu cation in Mg-samples. This could be explained by the incurporation of smaller Cu^{2+} (0.073 nm) as compared to Zn^{2+} (0.074 nm), and incorporation of larger Cu^{2+} when compared to Mg^{2+} (0.072 nm). Additional differences in c values were attributed to the reduction of interlayer interaction due to differences in local charge density after Cu incorporation. These small differences in a and c values indicated successful Cu^{2+} incorporation into cationic layers, also triggering a slight structural distortion.[16] By subtracting the brucite-like layer thickness (0.48 nm) from c' values, interlayer thickness occupied by carbonate was obtained.[17]

The d_p values (25.4–10.15 nm) depended on the sample composition: ZnAl–LDH > ZnCuAl–LDH > MgAl–LDH > MgCuAl–LDH. The d_p decrease after the Cu incorporation for both Zn- and Mg-samples, suggested that Cu incorporation inhibited the growth of crystallites. XRD analysis of Zn-calcined samples revealed dominate ZnO phase indexed as the hexagonal (wurtzite) structure and their lattice parameters (Table II) were calculated as:[14]

$$a = 2\times3^{-0.5}d_{110} \quad (7)$$

$$c = 2d_{002} \quad (8)$$

Considering the relation of reflections and structural parameters of calcined Zn-samples, the c/a ratio had values around 1.6 corresponding to the close-packed wurtzite structure. For Mg-calcined samples lattice parameter (Table II) was calculated as:[18]

$$a = dx(h^2 + k^2 + l^2)^{0.5} \quad (9)$$

The d_p of all calcined samples decreased in comparison to initial LDHs due to dramatic structural changes that occurred during calcination.[6]

The degree of LDH-sheet disorder was analysed by Raman spectroscopy, Fig. 2. The spectra revealed three distinct regions indicating that LDHs had the same features without any additional vibration bands. Similar properties could be explained by the presence of the doublet at 490 and 554 cm^{-1} that corresponded to transitional vibration modes EgT and EuT of M-OH planes typical for the brucite-like sheets[19]. Cu-samples retained lattice vibrational bands of the doublet, but with an intensity decrease due to the Jahn–Teller effect.[20] Distinctive peaks were also detected at 153 and 1063 cm^{-1} assigned to transitional and symmetric stretching vibration modes of intercalated carbonates.[20] The highest peak intensity for ZnAl–LDH sample suggested the highest degree of order in brucite-like sheets.

TABLE II. Lattice parameters, crystal structure and specific surface area of calcined samples

Parameter	ZnAl–C	ZnCuAl–C	Parameter	MgAl–C[a]	MgCuAl–C[a]
d_{100} / nm	2.8023	2.7845	d_{200} / nm	2.0976	–
d_{002} / nm	2.5983	2.5961	d_{220} / nm	1.4810	–
a / nm	3.2358	3.2152	a / nm	4.1921	–
c / nm	5.1967	5.1923	d_p / nm	3.58	3.16
c / a	1.606	1.615	S / m^2g^{-1}	231.8	128.1
d_p / nm	4.71	3.26			
S / m^2g^{-1}	84.2	90.3			

[a]Reflections overlapping-lattice parameters were not calculated

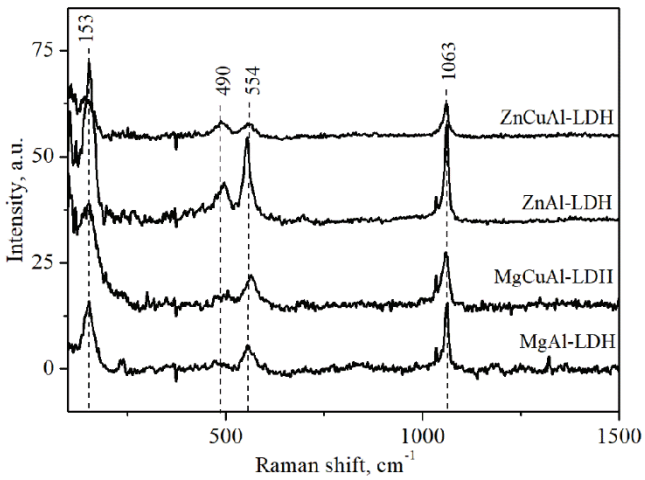

Fig. 2. Raman spectra for LDHs.

Textural characterization

Pore size distribution (PSD) curves demonstrated an overall wide monomodal distribution for LDH-samples and bimodal pore size distribution for cal-

cined samples (Fig. 3). All LDHs exhibited a wide pore size distribution. Calcination triggered the formation of smaller mesopores, as well as the increase of larger mesopores in the broad range, evidenced by broad peaks with shoulders towards lower and higher pore diameters for Mg-samples. Smaller mesopores probably originated from venting holes in the nanosheets, whereas larger mesopores correspond to pores formed between stacked laminar-nanosheets.[21]

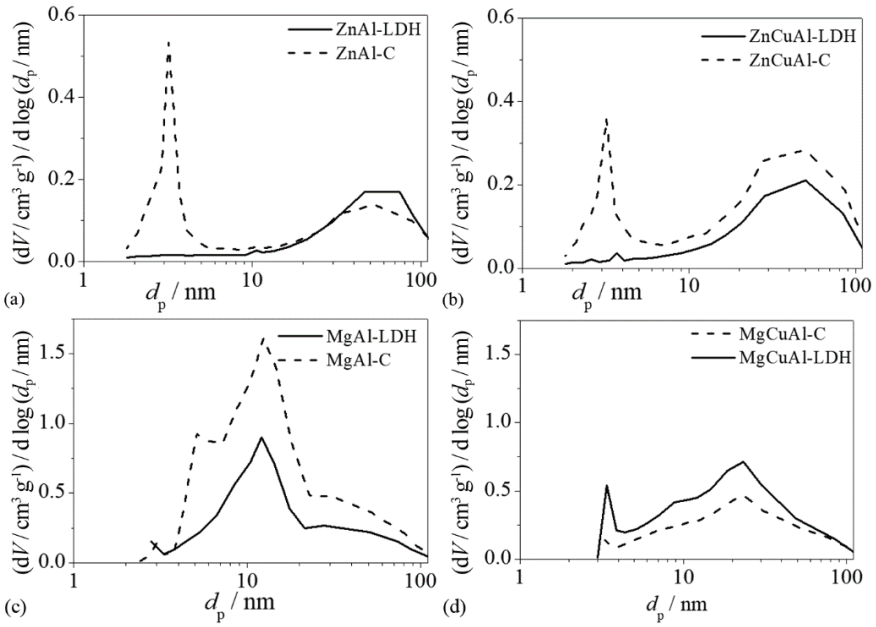

Fig. 3. Pore size distribution curves of: a) ZnAl-samples, b) ZnCuAl-samples, c) MgAl-samples and d) MgCuAl-samples.

Larger surface area of calcined samples (Tables I and II) was developed during thermal decomposition and evolution of CO_2 and H_2O. Cu-incorporation in Zn-samples, lead to the slight increase in surface area. On the contrary, MgAl–C had the highest surface area being almost twice as high as the specific surface area of MgCuAl–C sample, probably due to MgAl–C phase composition difference, where mixed-oxide phase and residues of parent LDH phase were detected. Textural characterization revealed hierarchical pore structure and developed specific surface area suggesting higher presence of active adsorption sites regarded as favourable for mass transfer enabling diffusion and fast transport of adsorbates in interconnected pore structure systems.[22]

Adsorption experiments

The effect of contact time on MO removal was investigated (time intervals: 30–60 min), Fig. 4. When compared to Zn-samples, Mg-samples showed higher

removal efficiency after 60 min in following order: MgCuAl–LDH > MgAl–LDH >> ZnCuAl–LDH > ZnAl–LDH probably because of larger specific surface areas, lower crystallinity and average crystallite size. Lower removal efficiency of ZnAl–LDH could be attributed to its highest degree of brucite-like sheets order and highest average crystallite size disabling the formation of structure disorder with higher surface energy such as adsorption sites.

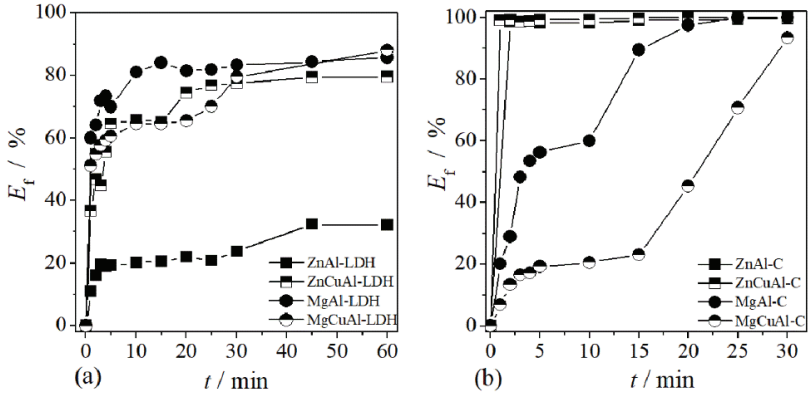

Fig. 4. MO removal efficiency for: a) LDHs and b) calcined samples.

Even higher removal efficiency was detected for calcined samples (Fig. 4b), where Zn-samples reached 100 % of dye removal (complete decolourization) almost instantly, whereas the same efficiency for Mg-samples occurred after 30 min. These results indicate that texture was not the limiting factor for removal efficiency and different adsorption efficiency could be assigned to other properties. Increased removal efficiency of Zn-calcined samples could be explained by the higher Zn electronegativity (electronegativity increase: Mg < Al < Zn < Cu) that enhanced the attractive forces between the positive layers and anionic dye molecules.[7] High removal efficiency could be clarified by the structural memory effect possible after calcination (T < 700 °C), forming non-stoichiometric mixed oxides with the ability to reconstruct LDH structure by the rehydration process.[23] Depending on metal components, formed mixed oxides exhibited different properties, such as electronegativity and alkalinity, initiating different interactions with MO during the rehydration process. These adsorption efficiency results are in accordance with similar research where authors stated that high removal efficiency is not only initiated by the developed surface area, but also through composition and structural diversity triggered by the memory effect.[7,23] XRD spectra for pristine LDHs and calcined samples after MO removal proved that structural memory effect was triggered during the removal process (Fig. 5).

XRD results, Table I, revealed no significant changes in the LDH structure, as well as in lattice parameters, of the pristine and rehydrated LDHs. Therefore,

the intercalation of MO ions into the LDH interlayer did not take place during the removal process. MO adsorption occurred on the external surface through electrostatic attraction[22] emphasizing surface properties of adsorbents.

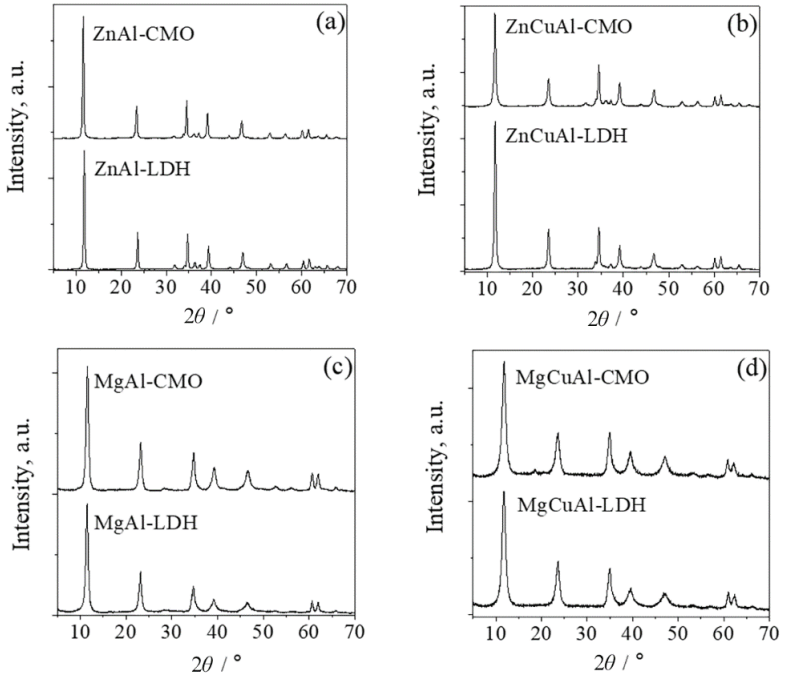

Fig. 5. XRD reflections of LDHs and CMO samples for: a) ZnAl-samples, b) ZnCuAl-samples, c) MgAl-samples and d) MgCuAl-samples.

The results of the kinetic study showed that pseudo-second order q_{e2} value was very close to the experimental q_e value, indicating good experimental data fit (Fig. 6, Table III).

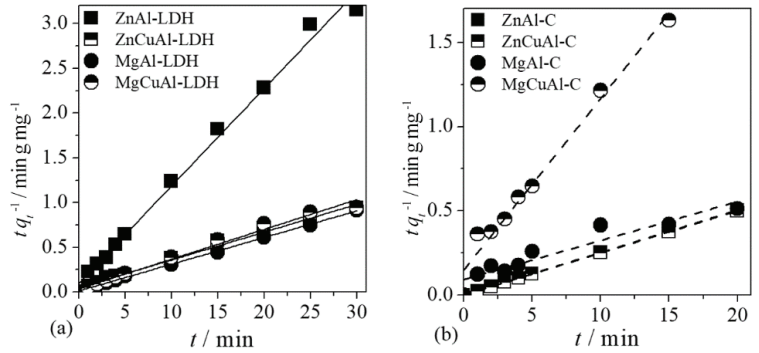

Fig. 6. Pseudo-second order model for: a) LDHs and b) calcined samples.

TABLE III. Pseudo-second order model parameters

Sample	q_e / mg g^{-1}	q_{e2cal} / mg g^{-1}	k_2 / g·mg^{-1}min^{-1}	R^2
ZnAl–LDH	13.76	13.966	0.0121	0.981
ZnCuAl–LDH	30.96	32.15	0.0206	0.997
MgAl–LDH	34.44	34.60	0.0373	0.999
MgCuAl–LDH	38	36.101	0.0092	0.995
ZnAl–C	39.96	40	0.2976	1
ZnCuAl–C	40	40	1.0420	1
MgAl–C	40	45.662	0.0049	0.961
MgCuAl–C	38	10.41	0.0457	0.993

The pseudo-second order kinetics is based on the solid-phase adsorption loading assumption that the rate-limiting step may be chemisorption (adsorbent––adsorbate interaction through electron sharing/exchanging). During the adsorption process adsorbate molecules bond to adsorbent solid surface in the following mass transfer steps:[24] *i*) external/film diffusion – adsorbate transport from bulk phase to external surface of the adsorbent; *ii*) sub-surface region diffusion; *iii*) pore diffusion (intra-particle diffusion) – migration of adsorbates from external surface to pores; *iv*) surface reaction – attachment of adsorbates to active sites situated in the internal surface of the adsorbent.

The limiting rate of the overall adsorption process was investigated using the IPD model where the intercept is related to the boundary layer thickness: larger C suggests that external diffusion is crucial rate-limiting step of the adsorption process[7] and the linear plot through the origin suggest IPD is sole rate-limiting step.[25] Multiple linear regimes for LDHs samples (Fig. 7a, Table IV) were observed: *i*) MO molecule diffusion to the external surface on numerous active ads-

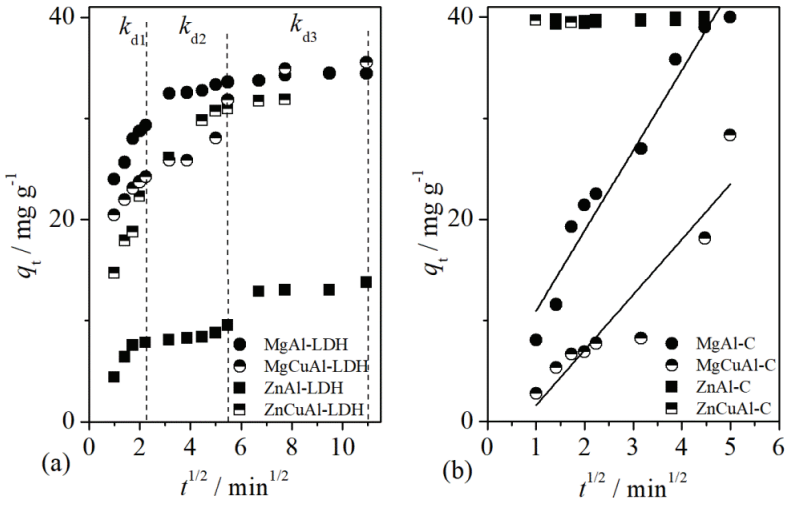

Fig. 7. IPD kinetic plot for: a) LDHs and b) calcined samples.

orption sites – steep linear regression (k_{d1}); *ii*) gradual adsorption reduction due to constrain of IPD (k_{d2}); *iii*) equilibrium stage (k_{d3}).[22,25]

TABLE IV. IPD model parameters

Parameter	ZnAl–LDH	MgAl–LDH	ZnCuAl–LDH	MgCuAl–LDH	MgAl–C	MgCuAl–C
k_{d1} / mg g^{-1} min$^{-1/2}$	4.342	5.007	8.503	3.314	7.934	5.466
C_{d1}	0.12	18.90	5.63	17.21	3.02	3.86
R^2_{d1}	0.994	0.978	0.939	0.994	0.096	0.878
k_d / mg g^{-1} min$^{-1/2}$	0.480	1.4673	2.582	1.307		
C_{d2}	6.64	26.27	17.99	21.31		
R^2_{d2}	0.912	0.948	0.992	0.935		
k_{d3} / mg g^{-1} min$^{-1/2}$	0.214	0.169	0.399	0.65		
C_{d3}	11.39	32.75	28.85	28.85		
R^2_{d3}	0.988	0.881	0.903	0.802		

Diffusion kinetic plot of calcined samples revealed different adsorption behaviour (Fig. 7b). For Zn-calcined samples no change in q_t *vs.* $t^{1/2}$ was observed and for Mg-calcined samples the plot did not pass through the origin indicating that IPD cannot be the sole rate controlling step, confirming a super-fast adsorbent-adsorbate interaction.

Stability experiments

In order to determine the stability, repeated adsorption experiments were carried out with re-used adsorbents (Fig. 8).

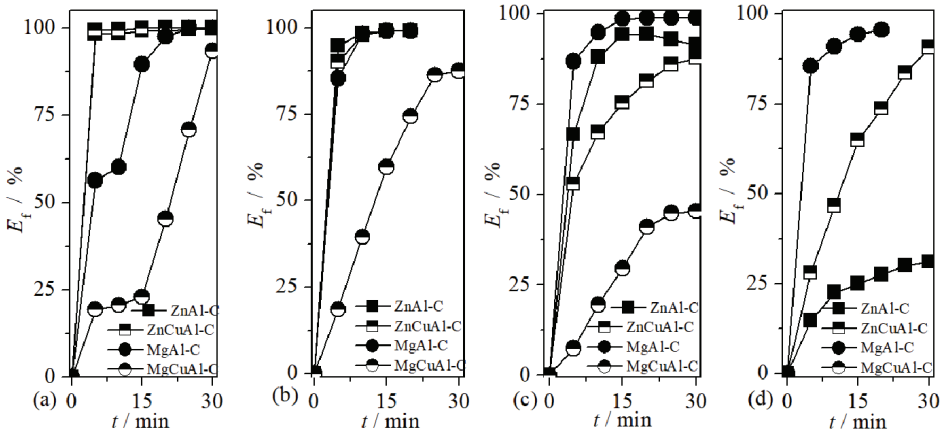

Fig. 8. Comparison of MO removal efficiency of all calcined samples in four adsorption cycles: a) I; b) II; c) III and d) IV.

After four consecutive adsorption cycles, the efficiency decrease was not substantial, indicating satisfactory stability and substantial adsorption capacity, probably due to their developed specific surface area providing a higher number of adsorption sites.

The results obtained from stability tests are consistent with research from the similar studies[8,26,27] where the decrease of adsorption capacity was detected after 3 or 4 cycles. This decrease was explained through structural characterisation of adsorbent proposing that one of important factors for the adsorption reduction was poor and decreased crystallinity of the LDH-like materials in structural reconstruction also detected in calcined samples.

CONCLUSION

The structural and textural properties of synthesized bimetal and trimetal LDH-based adsorbents were analysed (XRD, BET, BJH, Raman). The crystallinity, surface area, as well as pore structure varied in accordance with Cu-incorporation, thermal treatment and rehydration process. LDHs exhibited significant MO removal efficiency (30–87 % after 60 min). Complete MO decolourisation was achieved instantly for calcined Zn-samples and after 30 min for calcined Mg-samples. During the removal process structural memory effect was triggered in all calcined samples, indicating that the adsorption mechanism did not involve the MO ion intercalation into the LDHs, but occurred on the external surface through electrostatic attraction. The kinetic study revealed chemisorption as the rate-limiting step involving valence forces through sharing or exchanging of electrons between adsorbent and adsorbate. A super-fast adsorbent-adsorbate interaction makes these LDH-based adsorbents promising materials for MO removal.

Acknowledgments. Support from The Ministry of Education, Science and Technological Development of the Republic of Serbia (Contract No.451-03-9/2021-14/200134) and The Provincial Secretariat for Higher Education and Scientific Research (Contract No. 142-451--2341/2021-01/02) is highly acknowledged.

ИЗВОД

ПОБОЉШАНО ОТКЛАЊАЊЕ БОЈА ПРИМЕНОМ МУЛТИФУНКЦИОНАЛНИХ МАТЕРИЈАЛА НА БАЗИ СЛОЈЕВИТИХ ХИДРОКСИДА: АДСОРПЦИЈА И КИНЕТИКА

МИЛИЦА С. ХАДНАЂЕВ-КОСТИЋ, ТАТЈАНА Ј. ВУЛИЋ, ЂУРЂИЦА М. КАРАНОВИЋ и МАРИЈА М. МИЛАНОВИЋ

Технолошки факултет Нови Сад, Универзитет у Новом Саду, Вул. цара Лазара 1, 21000 Нови Сад

Двоструки слојевити хидроксиди (LDHs) се због повољних особина интензивно истражују у процесима отклањања органских боја. За потребе испитивања адасорпције метил-оранжа биметални (ZnAl и MgAl) и тријметални (ZnCuAl и MgCuAl) адсорбенти су синтетисани и термички третирани. Испитиван је утицај природе и садржаја градивног метала адсорбента на структурне (дифракција X-зрака, Раман анализа) текстуралне (нискотемпературна адсорпција азота) и адсорпционе карактеристике. Процес адсорпције, механизми и стабилност синтетисаних LDH и њихових калцинисаних мешовитих оксида је испитиван у циљу разјашњавања интеракције адсорбент–боја и оптимизације експерименталног дизајна. Сви LDH адсорбенси и адсорбенси на бази мешовитих оксида добијених калцинацијом LDH су показали високу ефикасност отклањања боје, нарочито мешовити оксиди са Zn код којих је дошло до потпуног обезбојавања (100 % уклањања боје) скоро моментално услед супер-брзе интеракције адсорбент–адсорбат.

Два могућа адсорпциона механизма иницирана међуповршинским феноменима су корелисана са структурним и текстуралним особинама, као и са феноменом реконструкције – „ефектом памћења“. Резултати представљају солидну базу за даља истраживања и дизајн адсорбената на бази LDH за уклањање метил оранжа, сагледавајући њихове повољне структурне и текстуралне особине, као и одличан адсорпциони капацитет.

(Примљено 28. фебруара, ревидирано 1. априла, прихваћено 8. априла 2022)

REFERENCES

1. H.-Y. Xu, B. L. Ping Li, *J. Serb. Chem. Soc.* **83** (2018) 1261 (https://doi.org/10.2298/JSC180501060X)
2. N. Li, Z. Chang, H. Dang, Y. Zhan, J. Lou, S. Wang, S. Attique, W. Li, H. Zhou, C. Sun, *Colloids Surfaces, A.* **591** (2020) 124507 (https://doi.org/10.1016/j.colsurfa.2020.124507)
3. T. Guan, L. Fang, Y. Lu, F. Wu, F. Ling, J. Gao, B. Hu, F. Meng, X. Jin, *Colloids Surfaces, A* **529** (2017) 907 (http://dx.doi.org/10.1016/j.colsurfa.2017.06.049)
4. M. Abniki, A. Moghimi, F. Azizinejad, *J. Serb. Chem. Soc.* **85** (2020) 1223 (https://doi.org/10.2298/JSC191011004A)
5. M. Hadnadjev-Kostic, T. Vulic, R. Marinkovic-Neducin, *Adv. Powder Technol.* **25** (2014) 1624 (https://doi.org/10.1016/j.apt.2014.05.015)
6. M. Hadnadjev-Kostic, T. Vulic, R. Marinkovic-Neducin, D. Loncarevic, J. Dostanic, S. Markov, D. Jovanovic, *J. Clean. Prod.* **164** (2017) 1 (https://doi.org/10.1016/j.jclepro.2017.06.091)
7. D. Bharali, R. Dekam, *Colloids Surfaces, A* **525** (2017) (https://doi.org/10.1016/j.colsurfa.2017.04.060)
8. K. Hassani, B. Beakou, D. Kalnina, E. Oukani, A. Anouar, *Appl. Clay Sci.* **140** (2017) 124 (https://doi.org/10.1016/j.clay.2017.02.010)
9. L. Zhang, J. Liu, H. Xia, D. Liu, Y. Qin, H. Wu, H. Li, N. Du, W. Hou, *Chem. Eng. J.* 250 (2014) 1 (https://doi.org/10.1016/j.cej.2014.03.098)
10. L. Wu, B. Peng, Q. Li, Q. Wang, X. Yan, K. Li, Q. Lin, *New J. Chem.* **44** (2020) 5293 (https://doi.org/10.1039/D0NJ00278J)
11. X. Cheng, X. Huang, X. Wang, D. Sun, *J. Hazard. Mater.* **177** (2010) 516 (https://doi.org/10.1016/j.jhazmat.2009.12.063)
12. N. Pathak, S. K. Gupta, L. Prajapat, S. K. Sharma, P. S. Ghosh, B. Kanrar, P. K. Pujariab, R. M.Kadam, *Phys. Chem. Chem. Phys.* **19** (2017) 11975 (https://doi.org/10.1039/C7CP01776F)
13. M. Jablonska, L. Chmielarz, A. Wegrzyn, K. Guzik, Z. Piwowarska, S. Witkowski, R. I. Walton, P. W. Dunne, F. Kovanda, *J. Therm. Anal. Calorim.* **114** (2013) 731 (https://doi.org/10.1007/s10973-012-2935-9)
14. A. A. A. Ahmed, Z. A. Talib, M. Z. Bin Hussein, *Appl. Clay Sci.* **56** (2012) 68 (https://doi.org/10.1016/j.clay.2011.11.024)
15. K. Morimoto, K. Tamura, N. Iyi, J. Ye, H. Yamada, *J. Phys. Chem. Solids* **72** (2011) 1037 (https://doi.org/10.1016/j.jpcs.2011.05.018)
16. L. Wu, B. Peng, Q. Li, Q. Wang, X. Yan, K. Li, Q. Lin, *New J. Chem.* **44** (2020) 5293 (https://doi.org/10.1039/D0NJ00278)
17. I. M. Ahmed, M. S. Gasser, *Appl. Surf. Sci.* **259** (2012) 650 (https://doi.org/10.1016/j.apsusc.2012.07.092)

18. R. A. B. Lima-Correa, C. S. Castro, A. S. Damasceno, J. M. Assaf, *Renew. Energy* **146** (2020) 1984 (https://doi.org/10.1016/j.renene.2019.08.047)
19. E.M. Seftel, R.G. Ciocarlan, B. Michielsen, V. Meynen, S. Mullens, P. Cool, *Appl. Clay Sci.* **165** (2018) 234 (https://doi.org/10.1016/j.clay.2018.08.018)
20. S. Kim, J. Fahel, P. Durand, E. André, C. Carteret, *Eur. J. Inorg. Chem.* (2017) 669 (https://doi.org/10.1002/ejic.201601213)
21. H. Zaghouane-Boudaiaf, M. Boutahala, L. Arab, *Chem. Eng. J.* **187** (2012) 142 (https://doi.org/10.1016/j.cej.2012.01.112)
22. C. Lei, X. Zhu, C. Zhu, B. Jiang, Y. Le, J. Yu, *J. Hazard. Mater.* **321** (2017) 801 (https://doi.org/10.1016/j.jhazmat.2016.09.070)
23. Z. Gao, K. Sasaki, X. Qiu, *Langmuir* **34** (2018) 5386 (https://doi.org/10.1021/acs.langmuir.8b00059)
24. K. L. Tan, B. H. Hameed, *J. Taiwan Inst. Chem. Eng.* **74** (2017) 25 (https://doi.org/10.1016/j.jtice.2017.01.024)
25. C. Peng, J. Dai, J. Yu, J. Yin, *AIP Advances* **5** (2015) 057138 (https://doi.org/10.1063/1.4921455)
26. Z.-M. Ni, S.-J. Xia, L.-G. Wang, F.-F. Xing, G.-X. Pan, *J. Colloid Interface Sci.* **316** (2007) 284 (https://doi.org/10.1016/j.jcis.2007.07.045)
27. Y. Guo, Z. Zhu,Y. Qiu, J. Zhao, *Chem. Eng. J.* **219** (2013) 69 (https://doi.org/10.1016/j.cej.2012.12.084).